Interaction of Jet in Hypersonic Cross Stream

J. S. Shang,* D. L. McMaster,† N. Scaggs,‡ and M. Buck§
Air Force Wright Aeronautical Laboratories, Wright-Patterson Air Force Base, Ohio

A jet stream issuing normally from both sharp- and blunt-nose ogive-cylinder configurations into a hypersonic flow was investigated by a side-by-side experimental and numerical simulation. At a hypersonic Mach number of 12, strong interaction between jet-induced and bow shock wave systems, the jet plume trajectory, and the separated-flow surface shear pattern were highlighted for basic understanding. After the numerical solution was verified with the experimental data, the flowfield topology was reconstructed. Several unique features of this inviscid-viscous interaction phenomenon of shock-wave formation, vortical flow structure, and jet plume were delineated.

Nomenclature

A = area of jet air supply line
D = diameter of jet aperture
M = Mach number
$\dot{m}$ = jet injection rate
P = pressure
Re = Reynolds number
T = temperature

Subscripts

j = condition of jet
0 = stagnation condition
∞ = freestream conditions

Introduction

A JET stream ejected into a crossflow is a frequently utilized technique for flight control of an aerospace vehicle and for supersonic combustion.[1-3] As a flight control device in the supersonic domain, the resultant force normal to the jet injecting surface can be many times greater than the reaction force generated by the jet itself. The effectiveness of the control system is relatively insensitive to flight altitude and yet free from heating problems.[2,3] Numerous investigations have been devoted to this intricate fluid dynamics phenomenon to determine similarity rules and to extract useful engineering information.[1-7] However, the basic understanding of the strong inviscid-viscous interaction, and specifically the structure of the induced separated flow region adjacent to the jet aperture, is very limited.

An analogy has frequently been drawn between the flow around a protuberance attached to a wall and the ejecting jet.[1,8,9] Indeed, the pressure-gradient-induced three-dimensional flow separation around the disturbance is similar. However, a fundamental difference exists in the topology of the flowfield; the stagnation region downstream of the jet is absent.[7] In a low-speed environment, the resulting flowfield adjacent to the surface is dominated by the jet stream, which induces a compression zone and pressure defect zone upstream and downstream of the jet.[10,11] Away from the jet issuing surface, the pressure difference and the interactive mixing of the two streams produce a rapid change in the direction of the jet plume. A pair of counter-rotating vortices is also formed contagiously downstream of the jet plume by the entrainment process. Farther downstream, the jet eventually aligns with the primary stream. Very few numerical simulations have been carried out to analyze this fundamental aerodynamic phenomenon.[5,12,13] Often only the jet trajectory was sought, and from it simplified analyses were devised to evaluate the characteristics of this aerodynamic phenomenon. Probably the only three-dimensional, compressible Navier-Stokes solution for the turbulent gas jet ejected into a high subsonic flow is due to Golbitz.[13] In the supersonic flow regime, no known numerical simulation of this strong interaction has been documented in the open literature.[12]

At supersonic and hypersonic conditions, the flowfield created by a jet normal to the flow is further complicated by the interaction of the bow shock wave and the jet-induced shock-wave system. This induced shock-wave system in turn generates a complex multistructure, three-dimensional, separated-flow region that surrounds the jet aperture. The exit jet expands rapidly, followed by deceleration, to form a Mach disk and deflects to realign with the primary stream.[2,6,7] Since we are venturing into an area that is largely unknown and uncertain, a parallel approach using experimental and numerical means is necessary. The experimental measurements were carried out in the AFWAL 20-in. blowdown wind tunnel operated at a nominal Mach number of 12 and a characteristic Reynolds number of 2.30×10^6/m. The surface oil film pattern, schlieren photographs of shock waves system, and selected surface pressures as well as pitot pressure surveys were collected for two mass injection rates. Numerical simulations using three-dimensional, mass-averaged Navier-Stokes equations were also performed. These calculations were conducted under the identical condition to that of the experiments, except that, at present, the numerical results are limited to the lower mass injection rate tested. In the present analysis, the experimental and calculated results are analyzed together to reconstruct the entire interacting phenomenon for basic understanding and possible future research emphasis.

Analysis

The experimental data were collected from a series of tests in a blowdown wind tunnel operated at a stagnation pressure of 5.516×10^3 kPa and a stagnation temperature of 964 K. Under these running conditions, the expanded air mixture in the test section is supersaturated but condensation-free. The model consists of an interchangeable sharp- and blunt-ogive forebody with an overall length of 25.4 cm and a 6.35-cm-diam cylindrical afterbody. The blunt nose is formed by a hemisphere with a radius of 1.27 cm. The ejected jet stream

Received June 30, 1987; revision received Aug. 30, 1987.

*Technical Manager. Associate Fellow AIAA.
†Visiting Scientist. Member AIAA.
‡Aerospace Engineer. Senior Member AIAA.
§Assistant Experimental Simulation. Associate Fellow AIAA.

was issued from a circular orifice of 0.635-cm diam located immediately downstream of the ogive forebody. The jet strength was controlled by the settling chamber pressure at room temperature. Two values of pressure were imposed for 344.7 and 689.5 kPa, resulting in nominal injection mass flow rates of 0.016 and 0.029 kg/s, respectively. These estimated mass flows contain some uncertainty. However, it is ascertained that the jet stream exits at a local supersonic Mach number and that the range of injection rate is nearly doubled for the cases tested.

A detailed description of the experimental instrumentation, procedures, and complete data set can be found in Ref. 14. The error analysis of pressure measurements (static and impact pressure), consistent with the past performance of this facility, indicated a data scattering band to be about 4%. A single-pass schlieren system was also used to investigate the interacting shock-wave structure. Finally, photographs of the surface oil-film pattern completed the experimental database.[14]

The numerical solutions were generated by solving the three-dimensional, mass averaged Navier-Stokes equations with a simple flux-gradient turbulent model.[15] Since the Reynolds number Re based on the model length is only 0.584×10^6, laminar-turbulent transition will most likely take place downstream of the interaction zone. The turbulence modeling was initiated accordingly. The numerical algorithm adapted in the present analysis is the MacCormack unsplit, explicit scheme.[16] This algorithm is easily coded for vector processing.[17] During the recent program modification process, the data-processing rate for 64-bit arithmetic with a vector length of 42 on a CRAY 2 computer attained a value of 3.2×10^{-5} s/grid point/iteration.

The mass-averaged Navier-Stokes equations and their associated conventional boundary conditions are well known. For our present purpose, only the unusual boundary condition for the jet-issuing control surface is included. The jet is assumed to expand isentropically in the air supply line from the sonic throat to the jet exit. For the present configuration, the area ratio $A/A^*=1.929$ yields a jet exit Mach number M_j of 2.156. Once the conditions for the settling chamber of the jet are specified (P_{0j}, T_{0j}), the physical properties of the exiting jet can be described by an isentropic expansion. Among several jet-issuing boundary conditions evaluated, the present formulation gave the most realistic description and systematic control of the rate of mass injection.

The numerical procedure is straightforward for the body conformal grid system. The singularity along the axis for the cylindrical (sharp-apex) or the spherical-cylindrical (blunt-nose) coordinate system is physically avoided by the grid and boundary conditions set across the axis of symmetry.[18] In our initial phase of research, the selected grid systems were limited by a CRAY XMP computer with a 2×10^6 word memory unit. Therefore, a $42\times45\times90$ and a $42\times45\times100$ grid system for the sharp- and blunt-nose configurations were used, respectively. The difference between the aforementioned grid systems is mostly in the distribution of grid points around the anticipated bow shock wave. A third computation for the blunt body employing an enriched grid system of $52\times90\times130$ was conducted on the CRAY 2 computer to improve the numerical resolution for the separated-flow region upstream of the jet. The three-dimensional grid system was constructed from a series of two-dimensional planes with a controlled clustering around the jet aperture. The peripheral gridpoints also were not uniformly distributed; the dense distribution was centered at the jet orifice. The minimum streamwise and circumferential mesh size was 0.1 of the jet diameter. The finest grid spacing normal to the body surface was 0.0008 cm. At the simulated hypersonic regime, the numerical procedure is susceptible to numerical oscillation generated by extreme gradients of flowfield and low ambient thermodynamic properties. In order to maintain numerical stability, higher than usual numerical damping values ($4<\beta<5.5$) and lower allowable time steps were enforced. The fourth-order difference dissipation term of MacCormack and Baldwin[17] was added to the formulation in the transformed computational space.

An unusually large number of iterations was needed for numerical convergence. For the cursory calculation ($42\times45\times90$), over 40 CRAY 2 cpu h were used to achieve an acceptable solution. The numerical convergence criterion is maintained by requiring a consecutive surface pressure change of less than 1% over a characteristic time scale.

Discussion of Results

The present discussion of results consists of three major areas. The first topic of discussion is focused on the similarities and differences between the jet interactions of the different nose configurations and injection rates tested. The second area of discussion is concentrated on the comparison of numerical results with experimental measurements. In the final section of discussion, a more detailed description of the flowfield topology will be derived from the numerical simulation.

Experimental Observations

In Fig. 1, a comparison of schlieren observations between the sharp-apex and blunt-nose configurations at different jet injection rates ($P_{0j}/P_{0\infty}=0.125$, $P_{0j}/P_{0\infty}=0.0625$) is presented. By nearly doubling the injection rate, the jet-induced shock-wave envelope displaces outwardly more than 20%. Visual quantification of the jet penetration height with respect to the jet stagnation pressure is extremely uncertain. Nevertheless, the limited present data do not support a formulation for jet penetration height by Zukoski et al.,[1] as anticipated. Specifically, these measured heights did not vary proportional to the square-root value of the jet stagnation pressure. However, for all of the test cases, the basic structures of the coalescence of λ-waves into the jet-induced shock, its intersection with the bow shock wave, and the rapid expansion of the jet plume are similar.

The surface oil-film patterns for both blunt- and sharp-nose configurations at the higher injection rate ($P_{0j}/P_{0\infty}=0.125$) are presented in Fig. 2. The injection-induced viscous-inviscid interactions produce an identical surface shear flow structure for both configurations. Multiple oil streaks of coalescence and divergence are present, indicating a complex multistructure, horseshoe vortical flow around the jet. Upstream of the jet, the saddle point of separation and nodal of attachment can also be easily recognized. In this region, the surface shear map bears a strong analogy to that of the shock-wave impingement on a body of revolution and flow over a cylindrical obstacle.[19,20] The shear line flows around the orifice and aligns with the primary stream downstream of the jet. The frequently cited twin counter-rotating vortex cores associated with a small cylindrical protuberance leave no clear footprint,[20] reflecting a significantly simpler flowfield topology for the jet interaction.

The pattern of surface oil film on both the sharp-apex and the blunt-nose configurations at the lower jet injection rate ($P_{0j}/P_{0\infty}=0.0625$) remains similar to that of the higher injection rate. However, there is an important but subtle difference near the plane of symmetry; the secondary oil streak accumulation is less pronounced. This observation reveals a possible bifurcation of the separated flow structure due to the reduced mass injection rate. Again, for both configurations tested, the lines of coalescence for the weaker jet retract uniformly toward the center of the jet aperture. The distance between the foremost upstream propagation of the oil streaks and the center of jet orifice decreases about 18% from results of higher mass expulsion. The embedded second line of oil accumulation shrinks at a slightly greater value of about 20%. These measurements hold for both configurations within experimental accuracy.

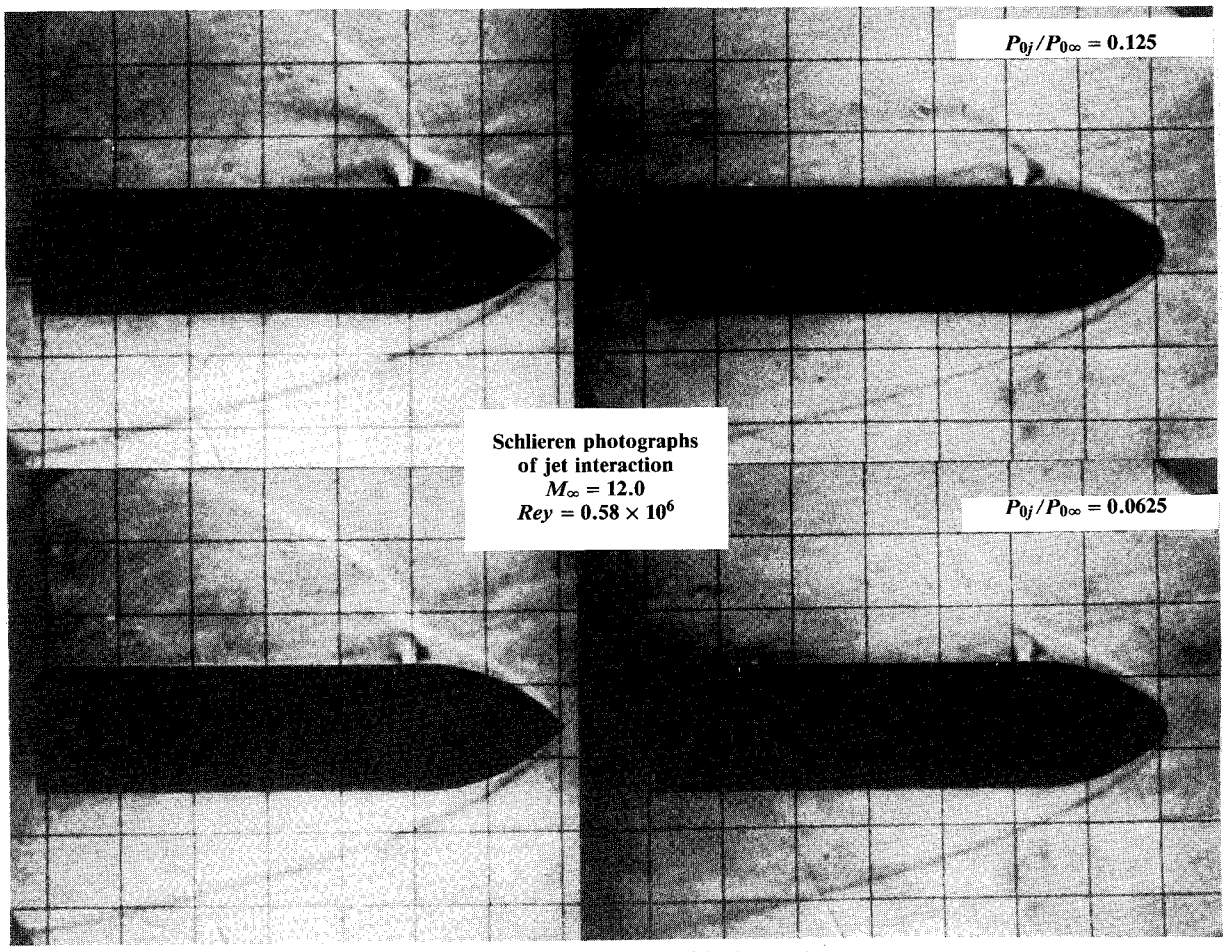

Fig. 1 Schlieren photographs of jet interaction.

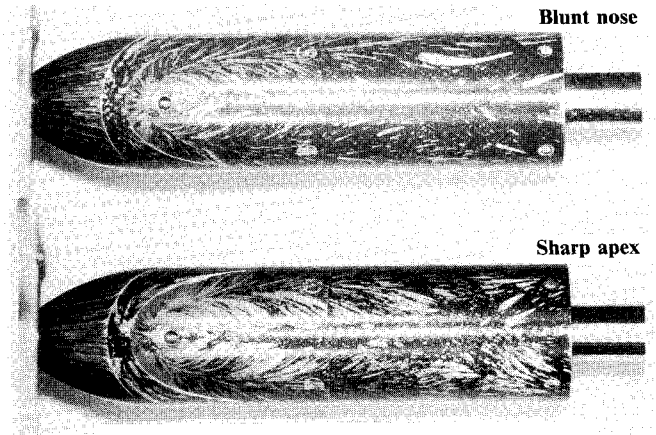

Surface oil film patterns for high injection rate
$M_\infty = 12.0$, $Rey = 0.58 \times 10^6$, $P_{0j}/P_{0\infty} = 0.125$

Fig. 2 Surface oil film patterns for high injection rate.

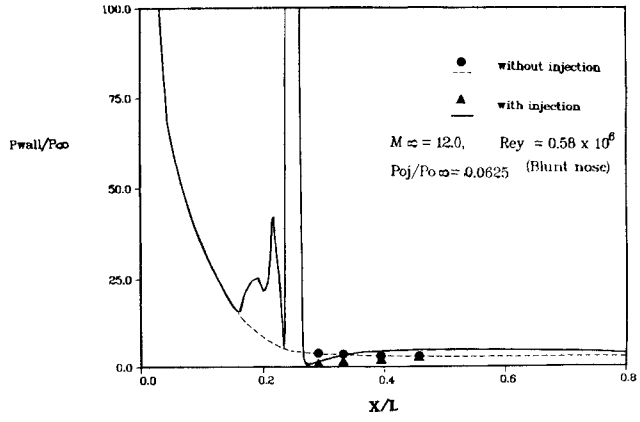

Fig. 3 Surface-pressure distributions in the plane of symmetry (blunt nose).

Comparsion of Numerical Results with Data

Based on the aforementioned observations, a substantially fewer number of calculations are required to provide a clear understanding of these interactive flowfields. Therefore, only the lower injection rate jet interactions were simulated by numerical means. A cursory computation was first performed for the sharp-apex configuration and followed by the numerical simulations for the blunt-nose body with refined mesh systems.

Comparisons of surface pressure distributions in the plane of symmetry containing the center of the jet with and without injection are depicted for both configurations in Figs. 3 and 4. Since the jet interaction is confined to the adjacent and downstream region of jet, the numerical results in the lower plane of symmetry are considered to be the no-injection situation.

The surface pressure distributions of both configurations, obtained by either experimental or numerical means, are almost identical within the region of strong inviscid-viscous interaction. Differences appear only in the nose region. For the blunt nose, the normalized pressure attains the stagnation value (Fig. 3), and the sharp apex yields the value for an attached shock envelope (Fig. 4). The surface pressure distribu-

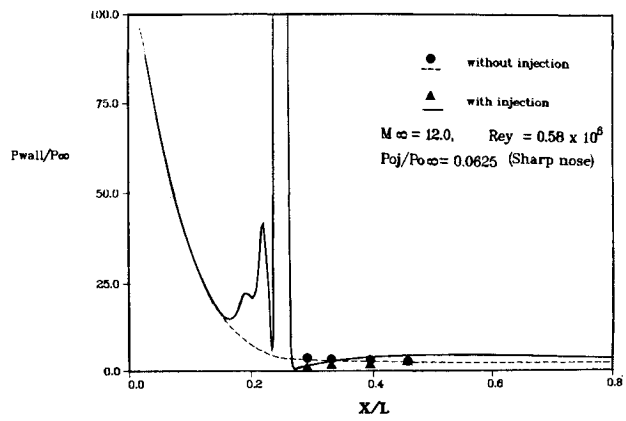

Fig. 4 Surface-pressure distributions in the plane of symmetry (sharp nose).

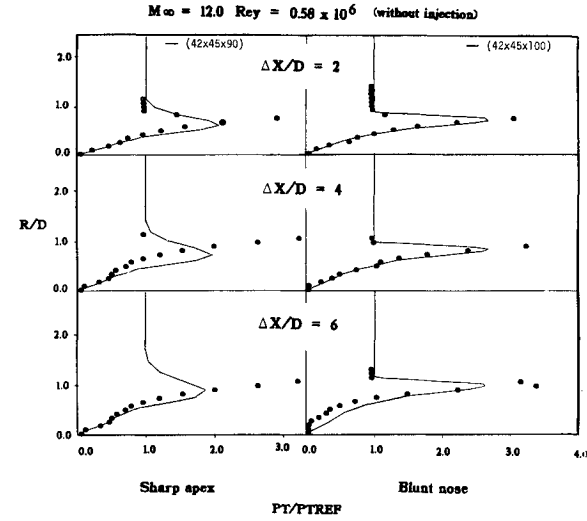

Fig. 5 Comparison of pitot-pressure profiles (without injection).

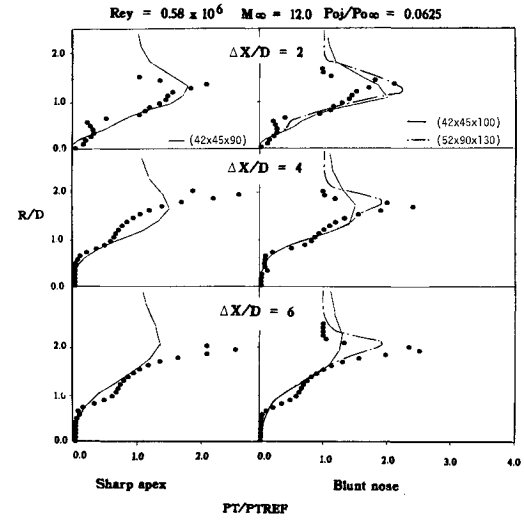

Fig. 6 Comparison of pitot-pressure profiles (with injection).

tions without injection simply indicate a monotonic expansion from either the sharp apex or the hemisphere to the afterbody. The agreement with experimental data is excellent. The surface pressure distributions in the plane of symmetry and containing the center of the jet aperture exhibit a wide range of variations. The continuous expansion from the nose region to the junction of the ogive forebody is still present. The upstream pressure propagation through the three-dimensional separated flow (horseshoe vortices) produces two pressure peaks, followed immediately by an expansion and a high-pressure plateau over the exhausting jet stream. Downstream of the jet, the surface pressure drops below the freestream value and then gradually recompresses to its asymptote. Both numerical results overpredict the experimental measurements. In this region, the static pressure attains the lowest value of the entire flowfield, and the numerical errors are most pronounced.

The specific comparisons of the pitot pressure profiles with and without the jet injection are presented in Figs. 5 and 6. Three sets of profile data were collected at two, four, and six times the jet aperture diameter downstream of its center. In Fig. 5, the comparison with data of no jet injection is given. The pitot pressure measurements of the sharp-apex and the blunt-nose bodies revealed a close similarity in shock-layer formation. The common features are apparently in the shock jump, its ensuing expansion toward the body, and the viscous dominant layer immediately adjacent to the body. However, a discernible difference is also indicated in the inner shock-layer structure, where the detached bow shock wave created a more extensive low-pitot-pressure region for the blunt body than that of the sharp-apex configuration. This upstream influence is most pronounced at the streamwise station $\Delta X/D = 4$, which is located downstream of the flow expansion around the junction of the ogive forebody and the cylindrical afterbody. In general, a reasonable agreement is reached between experimental data and numerical results. The same number of gridpoints (45) in the transverse direction was used for both computations. However, for the blunt-body calculation, the gridpoint distribution was clustered around the shock-wave envelope according to the experimental observation. A substantially better agreement between experimental data and numerical results in shock definition was obtained by adjustment of the gridpoint distribution.

The pitot pressure profiles with injection are presented in Fig. 6. The nearly identical measured pitot pressure profiles indicate that the injecting jetstream overwhelms completely the different upstream flow history for the two cases investigated. The numerical results, which suffer mostly from the lack of numerical resolution and possibly additional inadequate description of turbulence for jet mixing, yield only the essential features of the strongly interactive flow region. However, the discrepancy between data and calculations in the definition of shock-wave envelopes diminishes with increasing numerical resolution ($52 \times 90 \times 130$).

The comparisons of schlieren photographs with the density contour and the Mach number contour for the blunt- and the sharp-nose configurations are presented in Figs. 7 and 8, respectively. It is apparent that numerical results duplicated all of the main characteristics of the jet interactive flowfield. In the lower half-plane of symmetry opposite the jet orifice, the bow shock waves exhibit continuous and undisturbed formation from the nose to the afterbody. For the blunt-nose configuration, the shock wave is detached; thus, the shock envelope is displaced farther away from the body (Fig. 7). In the jet issuing plane, the jet-induced shock-wave system emanates from the upstream pressure propagation due to the three-dimensional separated flow. The λ shock wave formation upstream of the jet is clearly indicated in the density contours and is consistent with all experimental findings for supersonic streams.[1,2,6,7] The jet exiting from the aperture appears as a cylindrical obstacle normal to oncoming flow (Figs. 7 and 8). The deflection of the jet is obviously dependent on its momentum and thus the penetration height. Since the expanding jet is supersonic and the flow downstream of the shock envelope also expands rapidly to achieve supersonic Mach number, the Mach disk[2,6,7] frequently associated with supersonic jet inter-

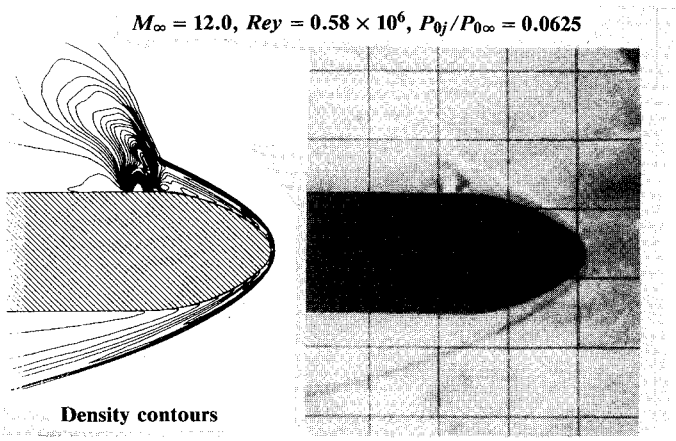

Fig. 7 Comparison of schlieren photograph with density contours.

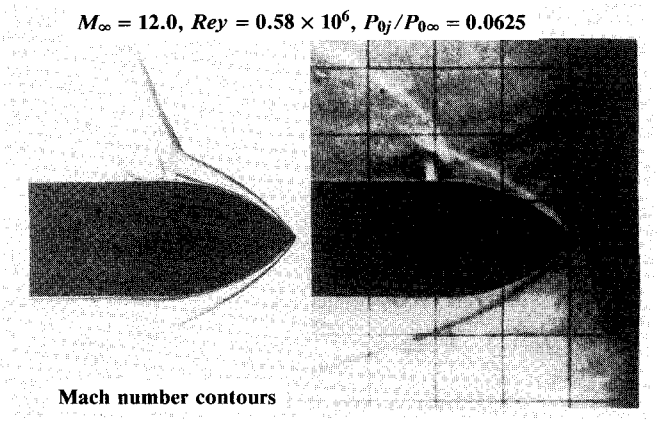

Fig. 8 Comparison of schlieren photograph and Mach number contours.

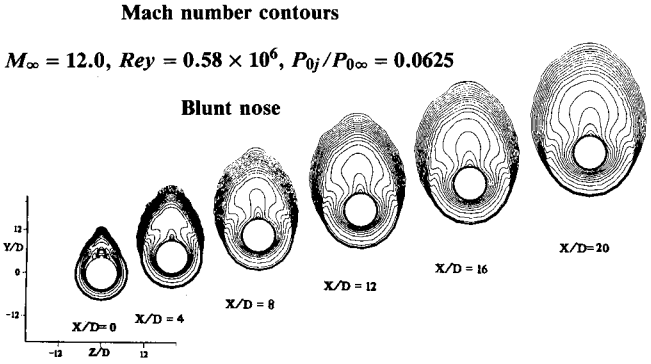

Fig. 9 Mach number contours of a few selected streamwise stations.

action does not exist for the investigated hypersonic flow. The jet-induced shock wave extends farther away from the body and eventually intersects the bow shock to form the final enveloping shock-wave system. All of these observations can be derived from the presentations in Figs. 7 and 8. In short, the numerical results and the experimental observations have attained some quantitative affinity between two entirely different means of data-acquisition processes.

The rather limited domain of dependence due to the jet injection is also indicated by Mach number contours in a few selected streamwise stations (Fig. 9). In the plane of injection and the subsequent streamwise stations, the shock-wave envelope is significantly distorted only in the quadrants that contain the jet aperture. Far downstream of the jet injecting station, the shock-wave envelope resembles that of a cylindrical body at a moderate angle of attack. Within the jet-induced shock-wave envelope, the subsonic domains are confined to shear layers adjacent to the solid surface and immediately downstream of the λ shock waves. Finally, there is no evidence of the Mach disk formation in the jet plume from either the experimental observation or the numerical results.

In Fig. 10, a comparison of the surface oil film and the limiting surface streamline pattern from numerical simulations of the body is presented. In the present analysis, the limiting surface streamline was depicted by the velocity vector field at the first nodes from the solid surface. The photograph was taken at the low jet injection rate. As was mentioned before, the basic oil-film topology is similar for the high and low mass injection rate. The lines of oil-streak accumulation and scavenging are similar. The affinity even includes the shear flow pattern around and behind the jet. The difference lies, however, in the physical dimensions of these surface phenomena and a relatively fainter inner oil-accumulation line in the vicinity of the symmetrical plane. At the low mass injection rate, two numerical simulations of the blunt-nose configurations were performed for the $42 \times 45 \times 100$ and $52 \times 90 \times 130$ grid point systems. The grid refinement of the latter was mainly in the upstream region of the jet orifice, where the gridpoint density was nearly double that of the coarse mesh system. From the experimental observation, one can quantify the foremost line of oil-film accumulation and the innermost line of scavenging to be 4 and 1.5 diam ahead of the center of the jet aperture, respectively. Both numerical solutions predicted these primary features of the separated flow within the experimental measuring uncertainty. However, some differences in the secondary structure of the surface phenomena are also noted. Specifically, the fine mesh calculation resolved distinctively the second line of surface shear accumulation, and the coarse mesh simulation yielded but a series of converging surface shear lines. Downstream of the jet aperture, numerical simulations of the surface phenomena are identical and duplicated the oil streaks on the model surface. The basic downstream structure is similar to that of the flow over a solid obstacle.[20] Therefore, no further elaboration will be offered here.

Topology of the Separated Flow Region

According to the limiting streamline theory[21-23] for three-dimensional flow separation, the convergence of skin-friction lines represents a necessary but not always sufficient condition for the occurrence of flow separation. However, there are few if any definitive illustrations with irrefutable measuring or computing accuracy to resolve this contention.[8,9,23] Even though the present insufficient numerical resolution produced the different topology of the simulated surface phenomena, these results appeared to be a meaningful illustration of the ambiguity in the study of flow separation. Particularly, a two-vortex, separated flow structure (the footprint on the surface is a single pair of oil-streak convergent and divergent lines) was observed for both the jet interaction at much lower injecting strength[7] and the flow upstream of a cylindrical protuberance.[20] By a shear coincidence, the simulated flow separation ($P_{0j}/P_{0\infty} = 0.0625$) is very close to the state of bifurcation. In this low shearing force region, the surface tension of the thin oil film impends its movement. It is doubtful that the accuracy of flow visualization technique can differentiate the subtle difference between a convergent and a converging oil streak. In this connection, the coarse grid computation reveals that this second line of oil accumulation correlates to the location where the velocity of the reverse flow underwent a significant reduction in magnitude. Thus, the present numerical results exhibit a possibility that the surface oil-film accumulation can also be generated by a sharp demarcation between high and low surface shear in a three-dimensional vortical structure.

$M_\infty = 12.0$, $Rey = 0.58 \times 10^6$, $P_{0j}/P_{0\infty} = 0.0625$

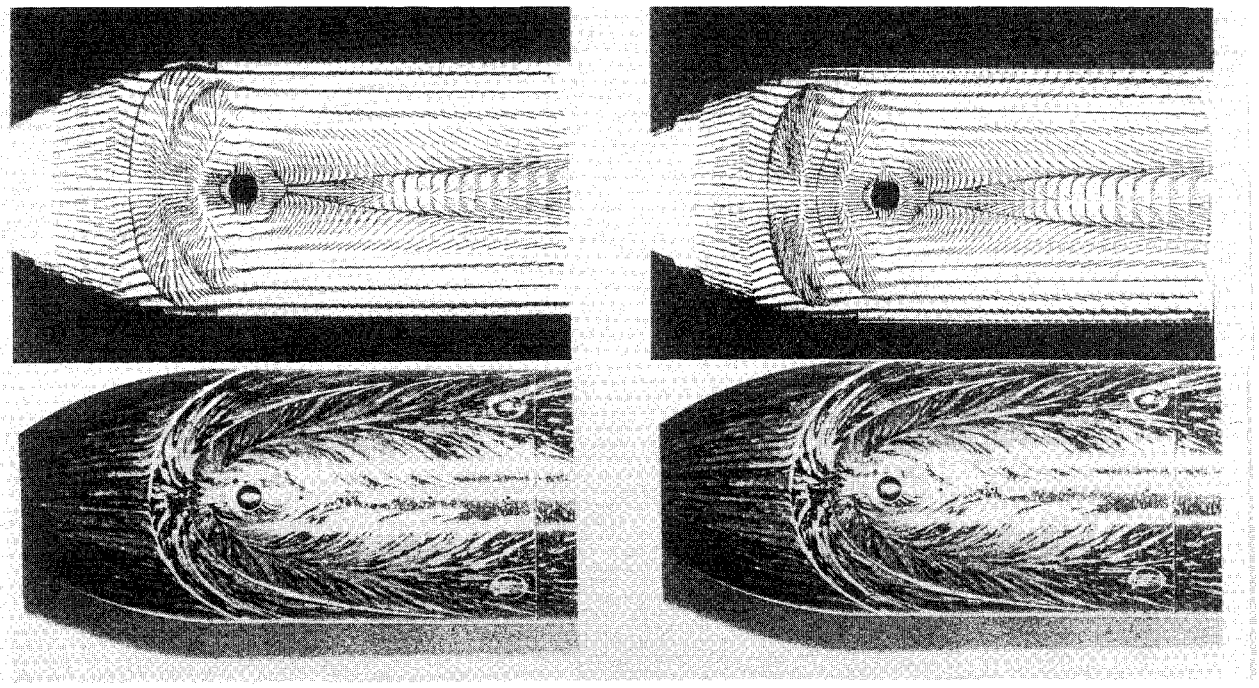

Fig. 10 Comparison of shear flow patterns.

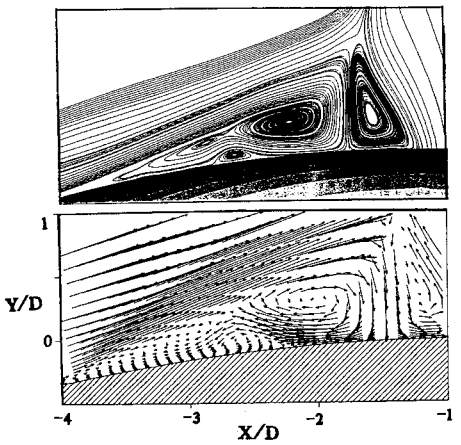

Fig. 11 Velocity vectors in the plane of symmetry.

Figure 11 depicts the velocity distribution and the derived particle trace of the fine mesh calculation. It is obvious that the horseshoe vortical formation consists of four separated vortices. Like that of the coarse mesh computation, the separated-flow structure is still dominated by the dominant pair of counterclockwise and clockwise vortices. The outstanding twin counter-rotating vortical formation is very similar to that of the horseshoe vortex ahead of a cylindrical obstacle[8,20] or a blunt fin.[9,24,25] However, the counterclockwise vortex entrained and reinforced by the jet is no longer a secondary structure, in contrast to the horseshoe vortical flow associated with a solid obstacle attached to a wall. These two vortices are separated by the fluid surface that eventually intersects the ogive surface ahead of the jet to form the primary nodal attachment.

A pair of additional secondary counter-rotating vortices is captured by the fine mesh point distribution. The secondary counterclockwise vortex attached to the solid surface and pinched the elongated reverse flow region into two clockwise vortices. Upstream of the primary nodal point of attachment, all three vortices originated from the saddle point of separation in the plane of symmetry. The fluid immediately adjacent to the wall spiraled into the primary clockwise vortex. The next layer of fluids similarly formed the forward-most secondary clockwise system. The rest of the entrained fluid constituted the secondary counterclockwise rotating vortex beneath the aforementioned two vortices and appeared as the secondary separated-flow region. Its footprint on the body surface is the second convergent line and the first divergence of the surface shear flow from the body nose (Fig. 10).

In the plane of symmetry, the local topological structure of the fine mesh computation indicated two more nodes of the vortices, two more half-saddle points of the secondary separated structure, and a saddle point partitioning the three neighboring vortices in comparison with that of the twin vortical formation. There is no change in the net balance of the two different types of singular points. Most importantly, it satisfies the topological rule of streamline in the two-dimensional section of the three-dimensional flows.[21-23]

Conclusion

A first, side-by-side experimental and numerical simulation of a jet issuing normally from surfaces of sharp- and blunt-nose ogive-cylinder configurations into a hypersonic flow was accomplished. For a wide difference of flow conditions and configurations, the jet interaction produced complicated and yet generally similar flowfield structures in formations of the horseshoe vortex and the exhaust jet plume trajectory. Under a presently investigated condition, the three-dimensional separated-flow region upstream of the jet indicated a quadruple counter-rotating horseshoe vortical structure, which is substantiated by the experimental observation. However, the numerical resolution requirement and the sufficient condition for the occurrence of the three-dimensional separated flow still requires future research.

Acknowledgment

Authors gratefully acknowledge the mutual support by William C. Golbitz of the Defense Nuclear Agency and the com-

puting resource provided by the Numerical Aerodynamic Simulation Project Office, NASA Ames Research Center.

References

[1]Zukoski, E. E. and Spaid, F. W., "Secondary Injection of Gases into a Supersonic Flow," *AIAA Journal*, Vol. 2, Oct. 1964, pp. 1689–1696.

[2]Zubkov, A. I. and Glagolev, A. I., "The Effect of Boundary Layer-Thickness and Transverse Curvature of the Surface on the Geometry and Forces Acting in the Separation Zone Produced by Injection of a Jet into a Supersonic Flow Over that Surface," *Fluid Mechanics—Soviet Research*, Vol. 8, Jan.–Feb. 1979, pp. 69–79.

[3]Werle, M. J., Driftmyer, R. T., and Shaffer, D. G., "Jet-Interaction-Induced Separation: The Two-Dimensional Problem," *AIAA Journal*, Vol. 10, Feb. 1972, pp. 188–193.

[4]Wooler, P. T., Buryhart, G. H., and Gallapher, J. T., "Pressure Distribution on a Rectangular Wing with a Jet Exhausting Normally into an Airstream," *Journal of Aircraft*, Vol. 4, Nov.–Dec. 1967, p. 537.

[5]Pantankar, S. V., Basu, D. K., and Alpay, S. A., "Production of the Three-Dimensional Velocity Field of a Deflected Turbulent Jet," *Transactions of ASME, Journal of Fluid Engineering*, Vol. 17, Dec. 1977, pp. 758–762.

[6]Avduevskii, V. S., Medvedev, K. I., and Polyanskii, V. S., "Interaction of a Supersonic Flow with a Transverse Jet Injected Through a Circular Aperture in a Plate," *Izvestiya, Akademii Nank SSSR, Mekhanika Zhidkoxtii Gaza*, No. 5, Sept.–Oct. 1970, pp. 193–197.

[7]Glagolev, A. I., Zubkov, A. I., and Panov, Y. A., "Supersonic Flow Past a Gas Jet Obstacle Emerging from a Plate," *Izvestiya Akademii, Nank SSSR, Mekhanjka Zhidkoxtii Gaza*, Vol. 2, March 1967, pp. 97–102.

[8]Peake, D. J. and Tobak, M., "Three-Dimensional Interaction and Vortical Flows with Emphasis on High Speeds," AGARD-AG-252, July 1980.

[9]Settles, G. E. and Dolling, D. S., "Swept Shock Wave/Boundary Layer Interactions," *AIAA Progress in Astronautics and Aeronautics: Tactical Missile Aerodynamics*, edited by M. Hensch and J. Nielsen, AIAA, New York, 1981.

[10]Keffer, J. F. and Baines, W. D., "The Round Jet in a Cross Wind," *Journal of Fluid Mechanics*, Vol. 15, Pt. 4, April 1963, pp. 481–496.

[11]Peake, D. J., "The Pressures on a Surface Surrounding a Jet Issuing Normal to Mainstream," NRC of Canada, Aeronautical Rept. LR-410, Nov. 1964.

[12]Shang, J. S., "Assessment of Numerical Solutions of the Compressible Navier-Stokes Equations," *Journal of Aircraft*, Vol. 22, May 1985, pp. 353–370.

[13]Golbitz, W. C., "Time-Dependent Navier-Stokes Solutions of a Turbulent Gas Jet Ejected from a Rectangular Orifice into a High Subsonic Cross Flow," Air Force Inst. of Technology, Ph.D. Dissertation, May 1980.

[14]Scaggs, N. E. and Buck, M. L., "Jet-Interaction Studies at Mach 12," Air Force Wright Aeronautical Labs., AFWAL-TM-86-231-FIMG, Sept. 1986.

[15]Baldwin, B. S. and Lomax, H., "Thin Layer Approximation and Algebraic Model for Separated Turbulent Flows," AIAA Paper 78-257, Jan. 1978.

[16]MacCormack, R. W., "The Effect of Viscosity in Hypervelocity Impact Cratering," AIAA Paper 69-354, Jan. 1969.

[17]Shang, J. S., Buning, P. G., Hankey, W. L., and Wirth, M. C., "Performance of a Vectorized Three-Dimensional Navier-Stokes Code on the CRAY-1 Computer," *AIAA Journal*, Vol. 18, Sept. 1980, pp. 1073–1079.

[18]Scherr, S. J. and Shang, J. S., "Three-Dimensional Body-Fitted Grid System for a Complete Aircraft," AIAA Paper 86-0428, Jan. 1986.

[19]Brosh, A., Kussay, M. I., and Hung, C. M., "An Experimental and Numerical Investigation of the Impingement of an Oblique Shock Wave on a Body of Revolution," *AIAA Journal*, Vol. 23, June 1985, pp. 840–846.

[20]Sedney, R. and Kitchens, C. W., Jr., "The Structure of Three-Dimensional Flows in Obstacle-Boundary Layer Interaction," *Flow Separation*, AGARD CP-168, Paper 37, 1975.

[21]Legendre, R., "Separation de L'ecoulement Laminaire Tridimensionnel," *Recherche Aeronautique*, Vol. 54, Nov.–Dec. 1956, pp. 3–8.

[22]Lighthill, M. J., "Attachment and Separation in Three-Dimensional Flow," *Laminar Boundary Layers*, edited by L. Rosenhead, Oxford Univ. Press, UK, 1963, pp. 72–82.

[23]Tobak, M. and Peake, D. J., "Topology of Three-Dimensional Separated Flows," *American Annual Review of Fluid Mechanics*, 1982, pp. 61–85.

[24]Hung, C. M. and Kordulla, W., "A Time-Split Finite-Volume Algorithm for Three Dimensional Flow Field Simulation," *AIAA Journal*, Vol. 22, Nov. 1984, pp. 1564–1572.

[25]Hung, C. M. and Buning, P. G., "Simulation of Blunt-Fin-Induced Shock Wave and Turbulent Boundary-Interaction," *Journal of Fluid Mechanics*, Vol. 154, May 1985, pp. 163–185.